AGU PUBLICATIONS

Geophysical Research Letters

RESEARCH LETTER
10.1002/2015GL064009

Key Points:
- Stereo photogrammetry can track dimensions and velocities of cloud thermals
- Stereo data can only be reconciled with known buoyancies if drag is substantial
- Wave drag, which is usually neglected, can generate the required drag

Supporting Information:
- Text S1, Figure S1, and Table S1

Correspondence to:
D. Romps,
romps@berkeley.edu

Citation:
Romps, D. M., and R. Öktem (2015), Stereo photogrammetry reveals substantial drag on cloud thermals, *Geophys. Res. Lett.*, *42*, 5051–5057, doi:10.1002/2015GL064009.

Received 26 MAR 2015
Accepted 29 MAY 2015
Accepted article online 4 JUN 2015
Published online 23 JUN 2015

Stereo photogrammetry reveals substantial drag on cloud thermals

David M. Romps[1,2] and Rusen Öktem[1,2]

[1]Department of Earth and Planetary Science, University of California, Berkeley, California, USA, [2]Earth Sciences Division, Lawrence Berkeley National Laboratory, Berkeley, California, USA

Abstract Stereo photogrammetry, which uses two synchronized cameras to measure three-dimensional positions, is applied here to ascertain whether drag plays a role in the ascent of cloud thermals. In particular, stereo cameras are used to measure the sizes and speeds of cloud thermals in Florida. Using the vertical momentum equation, it is found that a substantial amount of drag (a drag coefficient on the order of 1) is needed to match both the stereo-photogrammetric data and the known buoyancy of clouds from previous in situ measurements and large-eddy simulations. Empirical data on form drag and theoretical calculations of wave drag reveal that, for the observed Froude numbers of cloud thermals, a drag coefficient of about one is to be expected.

1. Introduction

The speeds of convective updrafts modulate many aspects of weather and climate. Fast updrafts can generate hail [*Danielsen et al.*, 1972], lightning [*Romps et al.*, 2014], and tornadoes [*Davies-Jones*, 1984] at the surface. Quickly rising clouds can also generate gravity waves [*Fovell et al.*, 1992] and clear-air turbulence [*Lane et al.*, 2012] that pose hazards for aircraft [*Lane et al.*, 2003]. Climatologically, the speed of updrafts in the upper troposphere controls the depth of convective overshooting [*Wang*, 2007] and, through injection of ice above the tropopause, moistening of the stratosphere [*Grosvenor et al.*, 2007]. But despite these important impacts of fast updrafts, little is known about the balance of forces that generates the updraft speeds. In particular, regarding the role of form drag and wave drag, the hypotheses range the gamut from drag being negligible (i.e., a drag coefficient of $c_d = 0$ [*Sherwood et al.*, 2013]) to drag being indispensible (i.e., drag entering the dominant balance with $c_d \approx 1$ [*Romps and Charn*, 2015]). Here we use cloud top trajectories measured by stereo photogrammetry to distinguish between these two paradigms. Note that the cloud-top speeds measured by stereo cameras, rather than the cloud-core speeds measured by Doppler radar, are the relevant speeds for form drag and wave drag since these sources of drag are generated by the relative flow of environmental fluid around the envelope of the ascending cloud.

In April of 2012, we established a pairing of cameras in Miami, Florida, to perform stereo photogrammetry of clouds. The two cameras paired up for this purpose are located 874 m apart and have overlapping fields of view of the clouds over Biscayne Bay [*Oktem et al.*, 2014]. The southern camera is part of a preexisting suite of instruments at the University of Miami's Rosenstiel School of Marine and Atmospheric Sciences. The northern camera, established in 2012, is located at the Marine and Science Technology (MAST) Academy, a Miami-Dade high school. With careful calibration of the two cameras, the disparities between the two vantage points can be used to reconstruct the three-dimensional position of any cloud feature that is visible to both cameras. The heights reconstructed by this method have been validated against data from colocated lidar for stratocumulus, altocumulus, and cirrocumulus [*Oktem et al.*, 2014].

Figure 1 shows a photograph from the MAST camera on 25 August 2013 at 12:28 UTC (8:28 A.M. local time). The curved edges of the photograph are caused by the postprocessing correction for optical barrel distortion. Front and center in this photograph is a mature cloud thermal sitting atop its cloudy wake. By calculating the width, height, and vertical velocity of these cloud thermals and using the buoyancy of cloud thermals known from in situ observations and large-eddy simulations, we can learn about the role of drag in the momentum budget of cloud thermals.

Figure 1. A photograph from the northern MAST camera taken on 25 August 2013 at 12:28 UTC (8:28 A.M. local time). This image shows a thermal rising front and center, along with a second thermal behind, and to its left.

2. Theory

In the usual formulation of the drag law, the magnitude of the drag force is written as $(1/2)c_d(\pi a^2)\rho w^2$, where πa^2 is the projected area of the sphere, ρ is the density of the fluid, and c_d is a dimensionless drag coefficient. We may think of this expression as a definition for c_d, which is defined by equating this expression with the net pressure perturbation force on the sphere due to form drag and wave drag. For a spherical thermal whose density is similar to its surroundings, this drag force generates an acceleration of the thermal equal to $(3c_d/8a)w^2$.

Entrainment can also generate an effective drag. The entrainment of air with zero momentum causes an effective deceleration that scales as w^2. Note that this is the same functional dependence as the standard drag law, so it can, in principle, be described by an effective c_d. In other words, an acceleration of the form $(3c_d/8a)w^2$ can, with an appropriate choice of c_d, accommodate all types of drag: form drag, wave drag, and entrainment drag. Studies have found, however, that the deceleration from entrainment is small [*Dawe and Austin*, 2011] and may be even slightly negative [*de Roode et al.*, 2012; *Sherwood et al.*, 2013]. Consistent with these findings, we will see below that form drag and wave drag are sufficient to explain the observations.

In addition to form drag and wave drag, there is one more source of pressure perturbation force that we must consider, and that is the pressure perturbation force caused by the acceleration of a thermal. When a thermal accelerates within a surrounding fluid, the fluid around the thermal must also accelerate. By Newton's third law, this means that the environmental fluid applies a force to the thermal anytime the thermal is accelerating, even if the thermal is momentarily motionless. This type of pressure perturbation force cannot be modeled with a drag law but can be modeled as an increase in the effective inertia of the thermal. For a spherical thermal whose density is similar to that of the environmental fluid, the thermal's effective inertia is 3/2 times its actual mass [*Batchelor*, 2005; *Romps and Kuang*, 2010].

Putting all of this together, we arrive at the vertical momentum equation for a spherical thermal,

$$\frac{3}{2}\frac{\mathrm{d}}{\mathrm{d}t}w = b - \frac{3c_d w^2}{8a}, \tag{1}$$

where a is the thermal's radius and b is the thermal's buoyancy. In the next section, we will attempt to interpret the stereo-photogrammetric data in the context of this equation. Of the variables in this equation, w and a are provided by the stereo-photogrammetric data, and the magnitude of b is known from in situ observations. With these observational inputs, equation (1) provides a powerful constraint on the value of c_d. Before moving

on to the next section, which performs this analysis, let us first consider the implications of equation (1) in the context of two competing hypotheses: $c_d = 0$ and $c_d \approx 1$.

The case of $c_d = 0$ is the "slippery thermal" paradigm advocated by *Sherwood et al.* [2013]. If $c_d = 0$ and assuming that $w = 0$ at the surface ($z = 0$), then the thermal's average buoyancy b between the surface and height z can be calculated exactly from the following expression for b in terms of w at height z:

$$b = \frac{3}{4z} w^2 \qquad \text{(slippery thermal)} . \tag{2}$$

Alternatively, the case of $c_d \approx 1$ is the "sticky thermal" paradigm advocated by *Romps and Charn* [2015]. If $c_d \approx 1$ and assuming that the thermal quickly reaches its terminal rise velocity, which is given by the balance between buoyancy and drag, then the buoyancy b can be calculated using the following expression in terms of w:

$$b = \frac{3c_d}{8a} w^2 \qquad \text{(sticky thermal)} . \tag{3}$$

In both cases, the inferred buoyancy is proportional to w^2, but the coefficient is quite different: roughly one over the height for the slippery thermal and roughly one over the diameter for the sticky thermal. For a cloud thermal with a diameter of 1 km at a height of 10 km, these two theories produce estimates for b that differ by an order of magnitude.

How fair is it to assume, in the $c_d \approx 1$ case, that the thermal has reached its terminal rise velocity? To find out, we can solve (1) for the case of constant buoyancy and $w = 0$ at $z = 0$. The solutions for $w(z, b)$ and $b(w, z)$ are

$$w = \sqrt{\frac{8ab}{3c_d}\left[1 - \exp\left(-\frac{c_d z}{2a}\right)\right]} \tag{4}$$

$$b = \frac{3c_d w^2}{8a}\left[1 - \exp\left(-\frac{c_d z}{2a}\right)\right]^{-1} . \tag{5}$$

Equation (5) smoothly connects the slippery-thermal solution in equation (2) for $c_d \ll 2a/z$ to the sticky-thermal solution in equation (3) for $c_d \gtrsim 2a/z$. Equation (4) makes clear that the thermal approaches its terminal velocity of $\sqrt{8ab/3c_d}$ over a length scale of $2a/c_d$. In particular, w is 80% of its terminal velocity by $z = 2a/c_d$. Taking $c_d = 1$, this implies that thermals have largely reached their terminal velocity after only traveling a distance equal to their diameter. This justifies our assumption of a steady state in the derivation of equation (3). In the next section, we will use (5) to diagnose the buoyancy of thermals for both the slippery and sticky hypotheses; the results are unchanged if (2) and (3) are used instead.

3. Stereo Data

For each of 32 unique cloud thermals observed at the Miami site during the months of April through September of 2013 and June through July of 2014, we collected a time series of cloud top height and a measurement of the thermal's radius. The cloud-top height measurements are collected from the first moment that the thermal's top is visibly rising (typically when the thermal emerges from a mass of relatively quiescent cloud) and continued until about 2 min before the cloud either starts to dissipate or form an anvil. Therefore, these measurements are collected during the cloud thermals' mature stage (as distinguished from the developing stage, which is typically hidden from view, and the dissipating stage, which is intentionally avoided).

Synchronized photographs are captured by the two cameras once every 30 s. Cloud thermals, which we envision as saturated quasi-spherical vortex rings sitting atop their cloudy wake [e.g., *Levine*, 1959; *Woodward*, 1959; *Blyth et al.*, 2005; *Damiani et al.*, 2006; *Sherwood et al.*, 2013; *Romps and Charn*, 2015], are identified in the stereo photographs as continuously rising cloud turrets. In each of the frames containing a cloud thermal, between one and four cloud top features are identified, those features are matched between the two images, and the heights of those features are then calculated using the principles of stereo photogrammetry. Each cloud thermal was observed for an average of 9 min. Contrary to the notion that moist convection comprises of steady state plumes, visual inspection of the time-lapse videos makes clear that moist convection comprises a sequence of short-lived thermals. An average of 41 cloud-top feature points was used

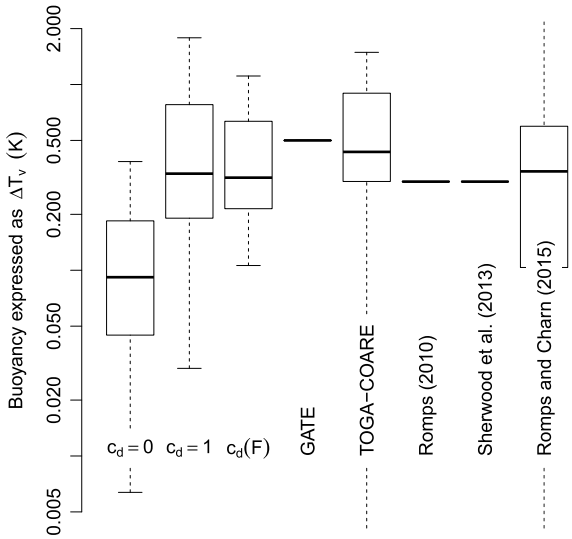

Figure 2. Box-and-whisker plots for equation (5) applied to the data in Table S1 using (first) $c_d = 0$, (second) $c_d = 1$, and (third) $c_d = c_{d,\text{form}} + c_{d,\text{wave}}$ with $c_{d,\text{form}} = 0.2$ and $c_{d,\text{wave}}$ given by equation (6). Buoyancy is quantified here as a loaded virtual potential temperature excess defined as b times $T_v = 270$ K and divided by 9.81 m s^{-2}. Also plotted are measurements of cloud-thermal buoyancy obtained from in situ measurements and large-eddy simulations; see the text for details.

to construct the time series of height for each cloud thermal. An estimate of the thermal's diameter was made by measuring the width of the cloud thermal at a height where its dimensions were most readily apparent, which was typically around halfway between z_i and z_f.

To a good approximation, the cloud thermals rise with constant velocity during the period of observation. This allows us to summarize the observed cloud-top time series by fitting a line to each time series using least-squares regression. Denoting the intercept and slope of the regression by z_r and w_r, the best fit line is $z = z_r + w_r t$. Denoting the times of the initial and final photograph pairs by t_i and t_f, we define a mean time $t_m = (t_i + t_f)/2$ and a mean height $z_m = z_r + w_r t_m$. The values of z_m, w_r, and the calculated radius a are the three pieces of data used to calculate buoyancy from equation (5). Table S1 in the supporting information reports these data for all 32 thermals that had reliable radius estimates.

4. Results

The first two box-and-whisker plots in Figure 2 show the distributions of buoyancies obtained from equation (5) using the data in Table S1 and either the slippery-thermal hypothesis ($c_d = 0$) or sticky thermal hypothesis ($c_d = 1$). The buoyancies in this plot are expressed as effective virtual temperature anomalies by multiplying the acceleration by a representative virtual temperature of $T_v = 270$ K and dividing by 9.81 m s^{-2}. With the slippery-thermal solution hypothesis ($c_d = 0$), the median buoyancy is 0.09 K, and the first and third quartiles are 0.04 K and 0.2 K, respectively. With the sticky-thermal hypothesis ($c_d = 1$), the median buoyancy is 0.3 K, and the first and third quartiles are 0.2 K and 0.8 K, respectively. Note that the third quartile (75th percentile) of the slippery thermal distribution is equal to the first quartile (25th percentile) of the sticky thermal distribution; these hypotheses give distinctly different predictions for the buoyancy. The box-and-whisker plot labeled $c_d(F)$ will be discussed in the next section.

Also shown in Figure 2 are the buoyancies of mature clouds reported from in situ observations and large-eddy simulations. A typical buoyancy in tropical maritime updrafts was found from in situ observations to be ~0.5 K during the Global Atmospheric Research Program Atlantic Tropical Experiment (GATE) [*Lawson and Cooper*, 1990]. In the Tropical Ocean–Global Atmosphere Coupled Ocean-Atmosphere Response Experiment (TOGA COARE), buoyancies were found to increase with vertical velocity [*Wei et al.*, 1998]. Using our w_r values to calculate buoyancies from the w-b relationship observed during TOGA COARE (using the data in Figure 9 of *Wei et al.* [1998] and assuming a constant buoyancy of 1.5 K for velocities greater than the largest value in that data) gives a median buoyancy of 0.4 K. In large-eddy simulations (LES) of tropical maritime convection, *Romps* [2010] found typical mean buoyancies of about 0.3 K for both shallow and deep convection, *Sherwood et al.* [2013] reported a mean cloud thermal buoyancy of 0.01 m s^{-2} (about 0.3 K), and the distribution of cloud thermal buoyancies from *Romps and Charn* [2015] has a median buoyancy of 0.4 K. All of these observed and modeled median buoyancies exceed the third quantile of the slippery-thermal distribution, indicating that the slippery-thermal hypothesis is incompatible with the data. In contrast, all of the observed and modeled median buoyancies lie within the first and third quantiles of the stick-thermal hypothesis and are clustered around the sticky-thermal median. In this analysis, we see that the sticky-thermal hypothesis easily reconciles the stereo-photogrammetric data with the existing buoyancy measurements, while the slippery-thermal hypothesis does not.

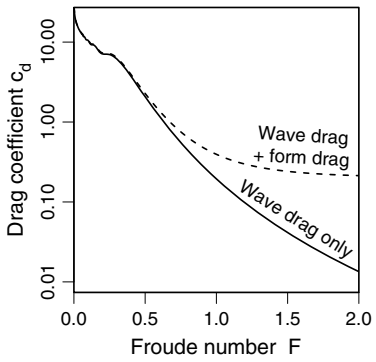

Figure 3. Plots of (solid) the wave drag coefficient $c_{d,\text{wave}}$ from equation (6) as a function of Froude number $F = w/Na$ and (dashed) the total drag $c_d = c_{d,\text{wave}} + c_{d,\text{form}}$ with $c_{d,\text{form}} = 0.2$.

5. Potential Sources of Drag

Section 2 described the three potential sources of drag that can contribute to an effective c_d: form drag, wave drag, and entrainment drag. Previous studies have presented evidence indicating that entrainment is not a significant source of drag [*de Roode et al.*, 2012; *Sherwood et al.*, 2013]. This leaves us with the following question: can form drag and wave drag generate the effective drag coefficient of $c_d \approx 1$ that the previous section demonstrated must be present? Let us consider these in turn, starting with form drag.

For a solid sphere or a spherical Hill's vortex ring moving through an inviscid fluid, there is no form drag because there is a fore-aft symmetry in the pressure field. In a real fluid, turbulence develops a wake at the rear of the sphere or vortex ring. This wake breaks the fore-aft symmetry, producing a net force that, by Bernoulli's law, is on the order of the projected area ($\sim a^2$) times the kinetic energy of the fluid ($w^2/2$). The constant of proportionality is called c_d, giving rise to the standard formulation of the drag law. Clearly, the fore-aft symmetry is broken for a cloud thermal: it trails a cloudy wake, as is evident in Figure 1. Therefore, cloud thermals are subject to form drag. At the highest Reynolds number for which form drag on a sphere has been studied in a laboratory setting, $c_{d,\text{form}}$ equals 0.2 [*Blevins*, 1992]. The form drag coefficient for highly turbulent cloud thermals is not known, so we will use this value as a best guess.

Form drag is present in both unstratified and stratified fluids, but stratified fluids also have wave drag caused by the transport of momentum away from the rising sphere or vortex by internal gravity waves. Equation (19) of *Warren* [1960] gives an expression for the wave drag on an object moving vertically through a stratified fluid. For a solid sphere, that expression can be integrated analytically and expressed in terms of a wave drag coefficient,

$$c_{d,\text{wave}} = 4\left[F\sin(2/F) - F^2\sin^2(1/F) - \text{Ci}(2/F) + \log(2/F) - 1 + \gamma\right], \tag{6}$$

where $F = w/Na$ is the Froude number, Ci is the cosine integral, and γ is the Euler-Mascheroni constant (see the supporting information for the derivation). The solid curve in Figure 3 plots this expression for $c_{d,\text{wave}}$, which increases monotonically with decreasing Froude number. For $F \leq 0.6$, $c_{d,\text{wave}}$ exceeds 1, which puts cloud thermals squarely in the "sticky" regime. To get an estimate of the combined effects of form drag and wave drag, we can define $c_d = c_{d,\text{form}} + c_{d,\text{wave}}$ using 0.2 for $c_{d,\text{form}}$. This total drag coefficient is plotted in Figure 3 as the dashed curve.

Figure 4 (top row) plots this theoretical wave drag in three different ways as a function of cloud-thermal radius a and cloud-top vertical velocity w. In the calculation of F from a and w, a buoyancy frequency of $N = 0.01\ \text{s}^{-1}$ is assumed. Figure 4 (top row, left column) plots the wave drag as an acceleration, which is equal to the wave drag force $[-(1/2)c_{d,\text{wave}}\rho\pi a^2 w^2]$ divided by the mass $[(4/3)\pi a^3\rho]$. Since the wave drag acts to decelerate the thermal's ascent, this acceleration is negative. Figure 4 (top row, middle column) plots the wave drag acceleration converted to an effective virtual temperature anomaly by multiplying the acceleration by $T_v = 270$ K and dividing by 9.81 m s^{-2}. Figure 4 (top row, right column) plots $c_{d,\text{wave}}$.

In Figure 4 (top row, left and middle columns), we see that the wave drag on a small thermal (i.e., with a radius $\lesssim$100 m) is practically zero for all ascent speeds; this fact was used by *Warren* [1960] to argue that wave drag is irrelevant for atmospheric thermals. For larger thermals, however, we see that the story is much more interesting. At a radius of 1 km, the wave drag force increases with vertical velocity at small speeds ($\lesssim$4 m s^{-1}) and decreases with vertical velocity at large speeds ($w \gtrsim 4$ m s^{-1}). At an ascent speed of 4 m s^{-1}, the wave drag peaks at about -0.02 m s^{-2}, which is equivalent to a virtual temperature anomaly of -0.6 K.

Figure 4 (bottom row) replicates Figure 4 (top row) but using the total drag obtained from $c_d = c_{d,\text{wave}} + c_{d,\text{form}}$ with $c_{d,\text{form}} = 0.2$. Overlaid on the panels in Figure 4 are circles denoting the radius a and velocity w of the 32

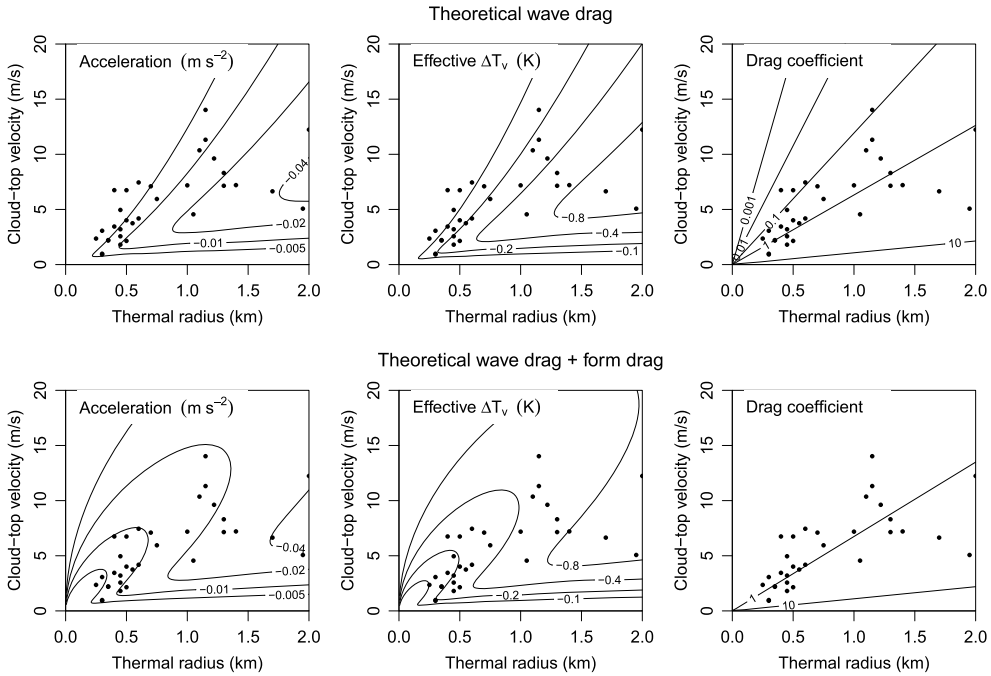

Figure 4. (top row) Using $c_{d,\mathrm{wave}}$ from equation (6), contours of (left column) the wave drag acceleration, calculated as $(1/2)c_{d,\mathrm{wave}}\pi a^2 w^2/[(4/3)\pi a^3]$; (middle column) the wave drag acceleration calculated as a contribution to virtual potential temperature, calculated as $(T_v/g)(1/2)c_{d,\mathrm{wave}}\pi a^2 w^2/[(4/3)\pi a^3]$ with $T_v = 270$ K; and (right column) the wave drag coefficient. (bottom row) Same but using the total drag coefficient $c_d = c_{d,\mathrm{wave}} + c_{d,\mathrm{form}}$ with $c_{d,\mathrm{form}} = 0.2$. The 32 observed thermals are overlaid as circles.

observed thermals. Assuming that all of the thermals have reached their steady-state terminal velocity, the buoyancy of the thermals must be equal to the total drag acceleration and so can be read off from Figure 4 (bottom row, middle). The median buoyancy calculated in this way from Figure 4 (bottom row, middle) is 0.3 K. This is the same as the median buoyancy calculated from the sticky-thermal hypothesis in the previous section and is in agreement with the in situ observations and large-eddy simulations. Note that the median buoyancy of 0.3 K calculated from Figure 4 is not calculated using the momentum equation as it was in the previous section but using empirical data for $c_{d,\mathrm{form}}$ and the wave drag formula in equation (6). The distribution of buoyancies calculated based on $c_d = c_{d,\mathrm{wave}} + c_{d,\mathrm{form}}$ is displayed in Figure 2 as the third box-and-whisker plot, which is labeled $c_d(F)$.

6. Summary and Discussion

We have used stereo photogrammetry to assess the importance of drag in the momentum equation for cloud thermals using two different methods. First, we combined three pieces of information—the ascent speeds and radii of cloud thermals measured with stereo cameras (Table S1), the vertical momentum equation (see equations (1) and (5)), and the buoyancies of cloud thermals measured from in situ observations and large-eddy simulations—to show that the sticky-thermal hypothesis ($c_d \approx 1$) fits the data well, while the slippery-thermal hypothesis ($c_d = 0$) is incompatible with the data; this is illustrated in Figure 2. Second, we combined three pieces of information—the ascent speeds and radii of cloud thermals from the stereo cameras (Table S1), the empirical value of form drag for a sphere at high Reynolds number (0.2), and a theoretical calculation of wave drag (equation (6))—to show that these give estimates of buoyancy that match the observations (see the third box-and-whiskers plot in Figure 2) and a c_d of about one (see Figure 4 (bottom row, right)). We conclude therefore that cloud thermals rising through clear air are sticky ($c_d \approx 1$).

From the arguments given here, wave drag should present a significant drag on cloud thermals rising through stably stratified clear air. On the other hand, thermals that rise through a large mass of cloudy air should feel little or no wave drag because the cloud mass has an effectively neutral or unstable stratification. For a large cloud mass with a moist-adiabatic temperature profile, N is zero, which implies $F = \infty$ and which,

by Figure 3 (see the "wave drag only" curve), tells us that $c_{d,\mathrm{wave}} = 0$. Therefore, while thermals rising through moist-adiabatic cloud masses should experience the same form drag and entrainment drag as in clear conditions, they should not experience wave drag.

Acknowledgments
This work was supported by the U.S. Department of Energy's Atmospheric System Research, an Office of Science, Office of Biological and Environmental Research program under contract DE-AC02-05CH11231. Thanks are due to the Marine and Science Technology (MAST) Academy, which hosted the northern camera, and to Paquita Zuidema for making images available from the southern camera, which is part of the Cloud-Aerosol-Rain Observatory (CARObs). The data used in this study are available in Table S1.

The Editor thanks four anonymous reviewers for their assistance in evaluating this paper.

References

Batchelor, G. K. (2005), *An Introduction to Fluid Dynamics*, Cambridge Univ. Press, Cambridge, U. K.
Blevins, R. D. (1992), *Applied Fluid Dynamics Handbook*, Krieger Company, Univ. of Michigan.
Blyth, A., S. Lasher-Trapp, and W. Cooper (2005), A study of thermals in cumulus clouds, *Q. J. R. Meteorol. Soc.*, *131*(607), 1171–1190.
Damiani, R., G. Vali, and S. Haimov (2006), The structure of thermals in cumulus from airborne dual-Doppler radar observations, *J. Atmos. Sci.*, *63*(5), 1432–1450.
Danielsen, E. F., R. Bleck, and D. A. Morris (1972), Hail growth by stochastic collection in a cumulus model, *J. Atmos. Sci.*, *29*(1), 135–155.
Davies-Jones, R. (1984), Streamwise vorticity: The origin of updraft rotation in supercell storms, *J. Atmos. Sci.*, *41*(20), 2991–3006.
Dawe, J. T., and P. H. Austin (2011), Interpolation of LES cloud surfaces for use in direct calculations of entrainment and detrainment, *Mon. Weather Rev.*, *139*(2), 444–456.
de Roode, S. R., A. P. Siebesma, H. J. J. Jonker, and Y. de Voogd (2012), Parameterization of the vertical velocity equation for shallow cumulus clouds, *Mon. Weather Rev.*, *140*(8), 2424–2436.
Fovell, R., D. Durran, and J. Holton (1992), Numerical simulations of convectively generated stratospheric gravity waves, *J. Atmos. Sci.*, *49*(16), 1427–1442.
Grosvenor, D., T. Choularton, H. Coe, and G. Held (2007), A study of the effect of overshooting deep convection on the water content of the TTL and lower stratosphere from Cloud Resolving Model simulations, *Atmos. Chem. Phys.*, *7*, 4977–5002.
Lane, T., R. Sharman, T. Clark, and H. Hsu (2003), An investigation of turbulence generation mechanisms above deep convection, *J. Atmos. Sci.*, *60*(10), 1297–1321.
Lane, T. P., R. D. Sharman, S. B. Trier, R. G. Fovell, and J. K. Williams (2012), Recent advances in the understanding of near-cloud turbulence, *Bull. Am. Meteorol. Soc.*, *93*(4), 499–515.
Lawson, R. P., and W. A. Cooper (1990), Performance of some airborne thermometers in clouds, *J. Atmos. Oceanic Technol.*, *7*(3), 480–494.
Levine, J. (1959), Spherical vortex theory of bubble-like motion in cumulus clouds, *J. Meteorol.*, *16*, 653–662.
Oktem, R., J. L. Prabhat, A. Thomas, P. Zuidema, and D. M. Romps (2014), Stereo photogrammetry of oceanic clouds, *J. Atmos. Oceanic Technol.*, *31*(7), 1482–1501.
Romps, D. M. (2010), A direct measure of entrainment, *J. Atmos. Sci.*, *67*(6), 1908–1927.
Romps, D. M., and A. B. Charn (2015), Sticky thermals: Evidence for a dominant balance between buoyancy and drag in cloud updrafts, *J. Atmos. Sci.*, doi:10.1175/JAS-D-15-0042.1.
Romps, D. M., and Z. Kuang (2010), Do undiluted convective plumes exist in the upper tropical troposphere?, *J. Atmos. Sci.*, *67*(2), 468–484.
Romps, D. M., J. T. Seeley, D. Vollaro, and J. Molinari (2014), Projected increase in lightning strikes in the United States due to global warming, *Science*, *346*(6211), 851–854.
Sherwood, S. C., D. Hernandez-Deckers, M. Colin, and F. Robinson (2013), Slippery thermals and the cumulus entrainment paradox, *J. Atmos. Sci.*, *70*(8), 2426–2442.
Wang, P. K. (2007), The thermodynamic structure atop a penetrating convective thunderstorm, *Atmos. Res.*, *83*, 254–262.
Warren, F. W. G. (1960), Wave resistance to vertical motion in a stratified fluid, *J. Fluid Mech.*, *7*, 209–229.
Wei, D., A. M. Blyth, and D. J. Raymond (1998), Buoyancy of convective clouds in TOGA COARE, *J. Atmos. Sci.*, *55*(22), 3381–3391.
Woodward, B. (1959), The motion in and around isolated thermals, *Q. J. R. Meteorol. Soc.*, *85*(364), 144–151.